

REDUCED PROJECTION METHOD FOR PHOTONIC MOIRÉ LATTICES

ZIXUAN GAO, ZHENLI XU AND ZHIGUO YANG

*School of Mathematical Sciences, MOE-LSC and CMA-Shanghai, Shanghai Jiao Tong University,
Shanghai 200240, China*

ABSTRACT. This paper presents a reduced projection method for the solution of quasiperiodic Schrödinger eigenvalue problems for photonic moiré lattices. Using the properties of the Schrödinger operator in higher-dimensional space via a projection matrix, we rigorously prove that the generalized Fourier coefficients of the eigenfunctions exhibit faster decay rate along a fixed direction associated with the projection matrix. An efficient reduction strategy of the basis space is then proposed to reduce the degrees of freedom significantly. Rigorous error estimates of the proposed reduced projection method are provided, indicating that a small portion of the degrees of freedom is sufficient to achieve the same level of accuracy as the classical projection method. We present numerical examples of photonic moiré lattices in one and two dimensions to demonstrate the accuracy and efficiency of our proposed method.

Key words. Quasiperiodic problems, Schrödinger eigenvalue problems, reduced projection method, Fourier method, basis reduction.

AMS subject classifications. 65N35, 65N22, 65F05, 35J05

1. INTRODUCTION

The quasiperiodic problems emerge naturally in a great many physical systems such as quasicrystals, many-body problems, and low-dimensional materials [1, 2, 3, 4, 5, 6, 7, 8, 9], and have found numerous applications in the areas of mechanics, acoustics, electronics, solid-state physics, and physics of matter waves [10, 11, 12, 13, 14]. Efficient and accurate numerical simulations of quasiperiodic problems play a critical role in exploring and utilizing novel material properties.

Though quasiperiodic systems are ubiquitous in mathematics and physics, the numerical method is not as straightforward as that of periodic systems. Specifically, quasiperiodic systems are space-filling ordered without decay and translational invariance [15]. In recent years, there has been a growing interest in the research of the optical properties of moiré lattices, a prototype of quasicrystals, as evidenced by notable studies in [16, 17, 18, 19] that have brought about significant breakthroughs in the field of optics. It is exhilarating to note that a localization-to-delocalization transition of eigenstates of moiré lattices in two dimensions is observed for the first time in both numerical simulations and experiments [2], which paves a new way of controlling light at will. However, the localization of eigenstates as well as the phase transition for a high-dimensional case is not well explored, due to the exceedingly huge degrees of freedom and computational cost required.

One of the widely used numerical approaches for solving these quasiperiodic problem is the periodic approximation method, also known as the crystalline approximant method [20, 21, 22], which approximates the quasiperiodic function via a periodic function in a certain supercell. Nevertheless, this method is proven to be of slow convergence and the simultaneous Diophantine approximation error does not decay uniformly as the size of the supercell gradually increases. In order to avoid the Diophantine error, considerable efforts have been made. Rodriguez *et al.* [23] introduced a numerical algorithm to compute the spectrum of photonic quasicrystals by raising the physical domain to higher dimensions. Jiang and Zhang [24, 25] proposed a projection method (PM), which treats a quasiperiodic function as a projection of a

higher-dimensional periodic function. The PM has the advantage of avoiding the simultaneous Diophantine approximation error and allowing for the convenient use of periodic boundary conditions for domain truncation. Despite the high accuracy, the PM requires solving problems in higher dimensions, leading to significant increases in the degrees of freedom (DOF), computational cost, and memory consumption. For instance, when solving a d -dimensional quasiperiodic eigenvalue problem, the projection method raises the d -dimensional quasiperiodic domain to an n -dimensional periodic domain (n is often twice as large as d). Correspondingly, the DOF of the PM is $O(N^n)$, where N is the number of Fourier grids in one direction. This makes the PM prohibitive for solving high-dimensional quasiperiodic problems.

In order to mitigate the curse of dimensionality and improve significantly the capability for solving the problem of high-dimensional photonic moiré lattices, we propose an efficient reduced projection method (RPM). This method is inspired by several pioneering works based on the PM for incommensurate problems. Wang *et al.* [26] characterizes the density of states of Schrödinger operators in the weak sense for the incommensurate system and proposes numerical methods based on the planewave discretization and reciprocal space sampling. Zhou *et al.* [27] propose a k -points sampling reduction technique under the planewave framework for the electronic structure-related eigenvalue problems of the incommensurate systems. Jiang *et al.* [28] propose a finite points recovery (FPR) method for non-smooth quasiperiodic systems. We highlight the novelties and main contributions of our work as follows:

- We propose a fast algorithm for the PM for solving d -dimensional Schrödinger eigenvalue problems describing photonic moiré lattices, which significantly reduces the DOF for the eigenvalue computation. The computational complexity of the proposed RPM for solving the first k eigenpairs using the Krylov subspace method is reduced from $O(kN^{2n})$ to $O(kN^{2(n-d)}D^{2d})$.
- We study the theoretical reliability of the RPM. We prove that the generalized Fourier coefficients of the eigenfunctions exhibit faster decay rate along a fixed direction associated with the projection matrix. Furthermore, a rigorous convergence analysis for the RPM is then presented to demonstrate the high efficiency of the proposed reduction approach.
- The RPM is applied to solve one-dimensional and two-dimensional photonic moiré lattice systems [2]. Numerical experiments showcase the effectiveness of the proposed RPM and demonstrate that it is promising for quasi periodic problems.

The rest of this paper is organized as follows. Section 2 presents some preliminary results on quasiperiodic functions. Section 3 proposes the RPM. By introducing the variational framework, the numerical method for quasiperiodic Schrödinger eigenvalue problems is described in details together with the error estimation. Section 4 presents numerical results to show the attractive performance of the algorithm. Section 5 makes conclusions with some closing remarks.

2. PRELIMINARIES ON QUASIPERIODIC FUNCTIONS

We denote \mathbb{R} , \mathbb{Q} , \mathbb{Z} , \mathbb{Z}^+ as the spaces of real, rational, integer, and positive integer numbers, respectively. Let $L^2(\Omega)$ and $H^m(\Omega)$ ($m \in \mathbb{Z}, m \geq 0$) be the usual square-integrable function space and Sobolev spaces following classic textbooks (see e.g. [29]). Given that there would be a frequent conversion between periodic and quasiperiodic functions, we adopt the subscripts “per” and “qp”, respectively, to differentiate the spaces they belong to and their associated inner products and norms. For instance, for a d -dimensional periodic function $F(\mathbf{z}) \in L^2_{\text{per}}([0, T]^d)$ with period T in each dimension (dubbed as “ T -periodic function”), its corresponding inner product and norm are denoted by

$$(F, G)_{\text{per}} = \frac{1}{T^d} \int_{[0, T]^d} F \bar{G} d\mathbf{z}, \quad \|F\|_{\text{per}} = \sqrt{(F, F)_{\text{per}}},$$

where \bar{G} is the complex conjugate of $G \in L^2_{\text{per}}([0, T]^d)$. For notational convenience, we omit the subscript “per” for periodic functions, if no ambiguity occurs.

To facilitate the development of efficient and accurate numerical methods for the quasiperiodic Schrödinger eigenvalue problem, we begin with a brief exposition of definition for quasiperiodic functions and their relevant properties (see monographs [30, 31] for comprehensive discussions).

Definition 2.1. A d -dimensional function $f(\mathbf{z})$ is quasiperiodic if there exists a $d \times n$ projection matrix \mathbf{P} such that $F(\mathbf{x}) = F(\mathbf{P}^\top \mathbf{z}) = f(\mathbf{z})$ is an n -dimensional periodic function, where all columns of \mathbf{P} are linearly independent over \mathbb{Q} . $F(\mathbf{x})$ is called the parent function of $f(\mathbf{z})$ with respect to \mathbf{P} .

It is worthwhile to point out that the projection matrix \mathbf{P} is not unique. Throughout the paper, \mathbf{P} is chosen such that $F(\mathbf{x})$ is 2π -periodic. Define the mean value of a d -dimensional quasiperiodic function $f(\mathbf{z})$ by

$$\mathcal{M}(f) = \lim_{L \rightarrow \infty} \frac{1}{|L|^d} \int_K f(\mathbf{z}) d\mathbf{z}, \quad (2.1)$$

where $K = \{\mathbf{z} \mid 0 \leq |z_i| \leq L, i = 1, \dots, d\}$. Correspondingly, one can define the square-integral quasiperiodic function space $L_{\text{qp}}^2(\mathbb{R}^n)$ as

$$L_{\text{qp}}^2(\mathbb{R}^n) := \{f(\mathbf{z}) \mid \mathcal{M}(f\bar{f}) < \infty\}, \quad (2.2)$$

with the inner product and norm defined by

$$(f, g)_{\text{qp}} = \mathcal{M}(f\bar{g}), \quad \|f\|_{\text{qp}} = \sqrt{(f, f)_{\text{qp}}}, \quad (2.3)$$

where f and g are quasiperiodic functions with respect to the same projection matrix \mathbf{P} .

It is well-known that $\{e^{i\langle \mathbf{k}, \mathbf{x} \rangle}\}_{\mathbf{k} \in \mathbb{Z}^n}$ serves as a complete orthonormal basis for $L_{\text{per}}^2([0, T]^n)$ such that for any $F(\mathbf{x}) \in L_{\text{per}}^2([0, T]^n)$, it has the Fourier series

$$F(\mathbf{x}) = \sum_{\mathbf{k} \in \mathbb{Z}^n} F_{\mathbf{k}} e^{i\langle \mathbf{k}, \mathbf{x} \rangle}, \quad F_{\mathbf{k}} = \frac{1}{T^n} \int_{[0, T]^n} F(\mathbf{x}) e^{-i\langle \mathbf{k}, \mathbf{x} \rangle} d\mathbf{x}, \quad (2.4)$$

and there holds the Parseval's equality $\|F\|^2 = \sum_{\mathbf{k} \in \mathbb{Z}^n} |F_{\mathbf{k}}|^2$. Lemma 2.1 relates the decay rate of Fourier coefficients with the regularity of a function (see [32, p.196]).

Lemma 2.1. Let $m \in \mathbb{Z}^+$, suppose $F(\mathbf{x}) \in H_{\text{per}}^m([0, T]^n)$, then

$$|F_{\mathbf{k}}| \leq (\sqrt{n})^m T^{-n} |\mathbf{k}|^{-m} |F|_{m, \text{per}}, \quad |F(\mathbf{x})|_{m, \text{per}}^2 = \sum_{\mathbf{k} \in \mathbb{Z}^d} \|\mathbf{k}\|_2^{2m} |F_{\mathbf{k}}|^2. \quad (2.5)$$

Quasiperiodic function also has the generalized Fourier series and Parseval's equality. One readily verifies $\{e^{i\langle \mathbf{q}, \mathbf{z} \rangle}\}_{\mathbf{q} \in \mathbb{R}^d}$ forms a normalized orthogonal system as

$$(e^{i\langle \mathbf{q}_1, \mathbf{z} \rangle}, e^{i\langle \mathbf{q}_2, \mathbf{z} \rangle})_{\text{qp}} = \delta_{\mathbf{q}_1, \mathbf{q}_2}, \quad \mathbf{q}_1, \mathbf{q}_2 \in \mathbb{R}^d, \quad (2.6)$$

where $\delta_{\mathbf{q}_1, \mathbf{q}_2}$ is the Dirac delta function. Thus, one can define the Fourier transform of the quasiperiodic functions, also called the Fourier-Bohr transformation (see [30]), as

$$\mathcal{F}_{\text{qp}}\{f\}(\mathbf{q}) = \mathcal{M}(f(\mathbf{z}) e^{-i\langle \mathbf{q}, \mathbf{z} \rangle}), \quad (2.7)$$

Correspondingly, one has the generalized Fourier series of the quasiperiodic function and the Parseval's equality in Lemma 2.2.

Lemma 2.2. (see [30]) Any d -dimensional quasiperiodic function $f(\mathbf{z})$ has generalized Fourier series

$$f(\mathbf{z}) = \sum_{\mathbf{q} \in \mathbb{Z}[\text{col}(\mathbf{P})]} f_{\mathbf{q}} e^{i\langle \mathbf{q}, \mathbf{z} \rangle}, \quad \mathbb{Z}[\text{col}(\mathbf{P})] := \{\mathbf{q} \mid \mathbf{q} = \mathbf{P}\mathbf{k}, \mathbf{k} \in \mathbb{Z}^n\}, \quad (2.8)$$

where $f_{\mathbf{q}} = (u, e^{i\langle \mathbf{q}, \mathbf{z} \rangle})_{\text{qp}}$ is called the \mathbf{q} th generalized Fourier coefficient of $f(\mathbf{z})$. In addition, there holds the Parseval's equality:

$$\|f\|_{\text{qp}}^2 = \sum_{\mathbf{q} \in \mathbb{Z}[\text{col}(\mathbf{P})]} |f_{\mathbf{q}}|^2. \quad (2.9)$$

Correspondingly, one can define the Sobolev spaces $H_{\text{qp}}^m(\mathbb{R}^d)$, $m \in \mathbb{Z}^+$ for quasiperiodic functions

$$H_{\text{qp}}^m(L_{\text{per}}^2(\mathbb{R}^d)) = \{f(\mathbf{z}) \in \mathbb{R}^d, \|f(\mathbf{z})\|_{m,\text{qp}} < \infty\}, \quad (2.10)$$

and its associated norm and semi-norm,

$$\|f(\mathbf{z})\|_{m,\text{qp}}^2 = \sum_{\mathbf{q} \in \mathbb{Z}[\text{col}(\mathbf{P})]} (1 + \|\mathbf{q}\|_2^{2m}) |f_{\mathbf{q}}|^2, \quad |f(\mathbf{z})|_{m,\text{qp}}^2 = \sum_{\mathbf{q} \in \mathbb{Z}[\text{col}(\mathbf{P})]} \|\mathbf{q}\|_2^{2m} |f_{\mathbf{q}}|^2. \quad (2.11)$$

Theorem 2.1 relates the generalized coefficients of quasiperiodic functions to the Fourier coefficients of its parent function ([15]).

Theorem 2.1. *Let $f(\mathbf{x})$ be a d -dimensional quasiperiodic function. There exists a parent function $F(\mathbf{x})$, which has a one-to-one correspondence between their Fourier coefficients, i.e.*

$$f(\mathbf{z}) = \sum_{\mathbf{q} \in \mathbb{Z}[\text{col}(\mathbf{P})]} f_{\mathbf{q}} e^{i\langle \mathbf{q}, \mathbf{z} \rangle}, \quad F(\mathbf{x}) = \sum_{\mathbf{k} \in \mathbb{Z}^n} F_{\mathbf{k}} e^{i\langle \mathbf{k}, \mathbf{x} \rangle}. \quad (2.12)$$

One has

$$F_{\mathbf{k}} = f_{\mathbf{q}}, \quad \text{iff } \mathbf{q} = \mathbf{P}\mathbf{k}. \quad (2.13)$$

By Theorem 2.1, one can denote the injective mapping $\psi : \mathbb{R}^d \rightarrow \mathbb{R}^n/[0, 2\pi]^n$ such that $\psi(\mathbf{z}) = \mathbf{P}^\top \mathbf{z} = \mathbf{x}$, and one can transform the quasiperiodic function into its periodic parent function. With a slight abuse of notation, we also regard ψ as an operator which maps the differential operator D in \mathbb{R}^d to the corresponding differential operator in \mathbb{R}^n , using the rules of partial differentiation. On the other hand, through the bijective mapping $\phi : \mathbb{Z}^n \rightarrow \mathbb{Z}[\text{col}(\mathbf{P})]$ s.t. $\phi(\mathbf{k}) = \mathbf{P}\mathbf{k} = \mathbf{q}$, one can obtain a one-to-one correspondence between the generalized Fourier coefficient of the quasiperiodic function and Fourier series of the periodic function.

3. REDUCED PROJECTION METHOD

In this section, we shall propose an efficient RPM for solving the problem of photonic moiré lattices, which is described by the following quasiperiodic Schrödinger eigenvalue problem [33]:

$$\mathcal{L}[u] := -\frac{1}{2}\Delta u(\mathbf{z}) + v(\mathbf{z})u(\mathbf{z}) = Eu(\mathbf{z}), \quad \mathbf{z} \in \mathbb{R}^d. \quad (3.1)$$

Here, $\mathbf{z} = (z_1, \dots, z_d)^\top$ is the physical coordinates in d dimensions, $v(\mathbf{z})$ is a quasiperiodic potential function, and $u(\mathbf{z})$ and E are respectively the eigenfunction and eigenvalue of the linear Schrödinger operator \mathcal{L} . The PM proposed by Jiang and Zhang in [24] serves as a viable way to solve quasiperiodic eigenvalue problems. The PM transforms the d -dimensional quasiperiodic problem (3.1) into its corresponding periodic one in n -dimensional space through the variable substitution $\psi(\mathbf{z}) = \mathbf{P}^\top \mathbf{z} = \mathbf{x}$. To be specific, it suffices to solve the periodic problem

$$-\frac{1}{2}\varphi(\Delta)U(\mathbf{x}) + V(\mathbf{x})U(\mathbf{x}) = EU(\mathbf{x}), \quad (3.2)$$

where $\varphi(\Delta)$ is given by

$$\varphi(\Delta) = \sum_{i=1}^d \sum_{j,l=1}^n P_{ij} P_{il} \frac{\partial^2}{\partial x_j \partial x_l}. \quad (3.3)$$

It is worthwhile to point out that due to the fact that operator $\varphi(\Delta)$ in Eq. (3.1) lacks ellipticity, the quasiperiodic Schrödinger operator has only continuous spectrum rather than discrete eigenvalues, as pointed out in [34]. Thus, when the resolution of the PM increases, the distribution of numerical eigenvalues gradually converges towards the density of states [26]. Consequently, a numerical eigenvalue of the PM can be viewed as approximation of a specific point within the spectrum.

Though the PM is a powerful and accurate numerical method for solving quasiperiodic Schrödinger eigenvalue problems, it suffers from the ‘‘curse of dimensionality’’. As the dimension is raised, the DOF required may become extremely large, making it computationally prohibitive and memory-intensive to

solve the quasiperiodic eigenvalue problem. For instance, a three-dimensional quasiperiodic problems with projection matrix of size 3×6 , the DOF to deal with is $O(N^6)$. This poses significant challenges in solving high-dimensional eigenvalue problems.

3.1. Decay rate of the generalized Fourier coefficients. To reduce the computational cost caused by dimension lifting, we propose a highly efficient RPM to tackle this issue. The RPM is based on the fact that the generalized Fourier coefficients of the eigenfunctions decay faster along a fixed direction of $\mathbf{P}\mathbf{k}$, which is presented in Theorem 3.2.

Theorem 3.2. *Let $u(\mathbf{z})$ be the eigenfunction of the d -dimensional quasiperiodic Schrödinger eigenvalue problem (3.1) corresponding to E , with $u_{\mathbf{q}}$ being its \mathbf{q} th generalized Fourier coefficient, and $v(\mathbf{z})$ and $V(\mathbf{x})$ being the quasiperiodic potential function and its parent function, respectively. Assume $V(\mathbf{x}) \in H_{\text{per}}^m([0, 2\pi]^n)$, ($m \in \mathbb{Z}$, $m \geq 0$). For any $\alpha \leq \max\{m - n + 2, 2\}$, there exists a constant C_α such that*

$$|u_{\mathbf{q}}| \leq C_\alpha \|\mathbf{q}\|_2^{-\alpha}, \quad (3.4)$$

where C_α depends on $m, n, \|\mathbf{P}\|, |V|_{\text{per}, m}$ and $\|v\|$.

Proof. Without loss of generality, let us set $\|u\|_{\text{qp}} = 1$. Define

$$g(\mathbf{z}) = v(\mathbf{z})u(\mathbf{z}) = \sum_{\mathbf{q} \in \mathbb{Z}[\text{col}(\mathbf{P})]} g_{\mathbf{q}} e^{i\langle \mathbf{q}, \mathbf{z} \rangle}, \quad \text{with} \quad g_{\mathbf{q}} = \sum_{\mathbf{p} \in \mathbb{Z}[\text{col}(\mathbf{P})]} v_{\mathbf{q}-\mathbf{p}} u_{\mathbf{p}}. \quad (3.5)$$

The weak form of Eq. (3.1) is to find $u \in H_{\text{qp}}^1(\mathbb{R}^d)$, such that

$$\frac{1}{2}(\nabla u, \nabla w)_{\text{qp}} + (g, w)_{\text{qp}} = E(u, w)_{\text{qp}}, \quad \forall w \in H_{\text{qp}}^1(\mathbb{R}^d). \quad (3.6)$$

For u , one has its generalized Fourier series,

$$u(\mathbf{z}) = \sum_{\mathbf{q} \in \mathbb{Z}[\text{col}(\mathbf{P})]} u_{\mathbf{q}} e^{i\langle \mathbf{q}, \mathbf{z} \rangle}. \quad (3.7)$$

Then by the orthogonality of $\{e^{i\langle \mathbf{q}, \mathbf{z} \rangle}\}$, one obtains from Eq. (3.6) that

$$Eu_{\mathbf{q}} = \frac{1}{2}|\mathbf{q}|^2 u_{\mathbf{q}} + g_{\mathbf{q}}, \quad \mathbf{q} \in \mathbb{Z}[\text{col}(\mathbf{P})]. \quad (3.8)$$

Then by the Parseval's identity and the fact that $\|u\| = 1$, one has

$$|g_{\mathbf{q}}| = \left| \sum_{\mathbf{p} \in \mathbb{Z}[\text{col}(\mathbf{P})]} v_{\mathbf{q}-\mathbf{p}} u_{\mathbf{p}} \right| \leq \frac{1}{2} \sum_{\mathbf{p} \in \mathbb{Z}[\text{col}(\mathbf{P})]} (v_{\mathbf{q}-\mathbf{p}}^2 + u_{\mathbf{p}}^2) = (\|v\|^2 + 1)/2. \quad (3.9)$$

By the assumption that $|\mathbf{q}|^2 > 4E$, it is direct to verify that

$$|E - |\mathbf{q}|^2/2| > |\mathbf{q}|^2/4. \quad (3.10)$$

Therefore, by Eqs. (3.8) and (3.9)

$$|u_{\mathbf{q}}| = \frac{|g_{\mathbf{q}}|}{|E - |\mathbf{q}|^2/2|} \leq 2(\|v\|^2 + 1)|\mathbf{q}|^{-2}. \quad (3.11)$$

By Eq. (3.8) again, one has

$$\left| E - \frac{1}{2}|\mathbf{q}|^2 \right| |u_{\mathbf{q}}| \leq \sum_{\mathbf{p} \in \Gamma_1} |v_{\mathbf{q}-\mathbf{p}}| |u_{\mathbf{p}}| + \sum_{\mathbf{p} \in \Gamma_2} |v_{\mathbf{q}-\mathbf{p}}| |u_{\mathbf{p}}|, \quad (3.12)$$

where $\Gamma_1 = \{\mathbf{p} | \mathbf{p} \in \mathbb{Z}[\text{col}(\mathbf{P})], |\phi^{-1}(\mathbf{q} - \mathbf{p})| > \|\mathbf{P}\|^{-1}|\mathbf{q}|/2\}$ and $\Gamma_2 = \mathbb{Z}[\text{col}(\mathbf{P})]/\Gamma_1$. We then estimate the summations in two parts, separately.

Estimate of the Γ_1 part. By the Parseval's identity and $\|u\| = 1$, one can obtain that for any \mathbf{q} , $|u_{\mathbf{q}}| \leq 1$. By the fact that $V(\mathbf{x}) \in H_{\text{per}}^m([0, 2\pi]^n)$ and Eq. (2.5), one obtains that

$$|V_{\phi^{-1}(\mathbf{q}-\mathbf{p})}| \leq \frac{n^{m/2}}{(2\pi)^n} |\phi^{-1}(\mathbf{q}-\mathbf{p})|^{-m} |V|_{\text{per},m}. \quad (3.13)$$

Then the bound

$$\begin{aligned} \sum_{\mathbf{p} \in \Gamma_1} |v_{\mathbf{q}-\mathbf{p}}| |u_{\mathbf{p}}| &\leq \sum_{\mathbf{p} \in \Gamma_1} |V_{\phi^{-1}(\mathbf{q}-\mathbf{p})}| \leq \frac{n^{m/2}}{(2\pi)^n} |V|_{\text{per},m} \sum_{\mathbf{p} \in \Gamma_1} |\phi^{-1}(\mathbf{q}-\mathbf{p})|^{-m} \\ &= \frac{n^{m/2}}{(2\pi)^n} |V|_{\text{per},m} \|\mathbf{P}\|^{-1} \sum_{|\mathbf{k}| > |\mathbf{q}|/2} |\mathbf{k}|^{-m} \end{aligned} \quad (3.14)$$

holds, where $\mathbf{k} \in \mathbb{Z}^n$. Then by the fact that

$$\sum_{|\mathbf{k}| > |\mathbf{q}|/2} |\mathbf{k}|^{-m} \leq \int_{|\mathbf{t}| > |\mathbf{q}|/2} |\mathbf{t}|^{-m} d\mathbf{t} = 2\pi \cdot 2^{n-2} \int_{|\mathbf{q}|/2}^{+\infty} |\mathbf{t}|^{n-m-1} d|\mathbf{t}| = \frac{2^{m-1}\pi}{m-n} |\mathbf{q}|^{n-m}, \quad (3.15)$$

one has

$$\sum_{\mathbf{p} \in \Gamma_1} |v_{\mathbf{q}-\mathbf{p}}| |u_{\mathbf{p}}| \leq C_1 |\mathbf{q}|^{n-m}, \quad (3.16)$$

where C_1 is a positive constant depending on $|V|_{\text{per},m}$, $\|\mathbf{P}\|^{-1}$, m and n .

Estimate of the Γ_2 part. By the Hölder's inequality with $1/\beta + 1/n = 1$,

$$\begin{aligned} \sum_{\mathbf{p} \in \Gamma_2} |v_{\mathbf{q}-\mathbf{p}}| |u_{\mathbf{p}}| &\leq \left(\sum_{\mathbf{p} \in \Gamma_2} |v_{\mathbf{q}-\mathbf{p}}|^2 \right)^{\frac{1}{\beta}} \left(\sum_{\mathbf{p} \in \Gamma_2} |v_{\mathbf{q}-\mathbf{p}}|^{\frac{\beta n - 2n}{\beta}} |u_{\mathbf{p}}|^n \right)^{\frac{1}{n}} \leq \max_{\mathbf{p} \in \Gamma_2} |v_{\mathbf{q}-\mathbf{p}}| \cdot \|v\|^{\frac{2}{\beta}} \left(\sum_{\mathbf{p} \in \Gamma_2} |u_{\mathbf{p}}|^n \right)^{\frac{1}{n}} \\ &\leq \|v\|^{\frac{2}{\beta} + \frac{1}{2}} \left(\sum_{\mathbf{p} \in \Gamma_2} |u_{\mathbf{p}}|^n \right)^{\frac{1}{n}}. \end{aligned} \quad (3.17)$$

For any $\mathbf{p} \in \Gamma_2$, one has

$$\|\mathbf{P}\|^{-1} |\mathbf{q}|/2 \geq |\phi^{-1}(\mathbf{q}-\mathbf{p})| \geq \|\mathbf{P}\|^{-1} |\mathbf{q}-\mathbf{p}|, \quad (3.18)$$

hence $|\mathbf{p}| > |\mathbf{q}|/2$. Because of Eq. (3.11), one can assume that the decay rate of $|u_{\mathbf{q}}|$ with $|\mathbf{q}|$ is α , that is, there exists a positive constant C_α independent with \mathbf{q} such that $|u_{\mathbf{q}}| \leq C_\alpha |\mathbf{q}|^{-\alpha}$. Then there exists a positive constant C_2 depending on n and such that

$$\sum_{\mathbf{p} \in \Gamma_2} |u_{\mathbf{p}}|^n \leq C_\alpha \sum_{\mathbf{p} \in \Gamma_2} |\mathbf{p}|^{-\alpha n} \leq C_\alpha |\Gamma_2| |\mathbf{q}/2|^{-\alpha n} \leq C_2 |\mathbf{q}|^{n-\alpha n}. \quad (3.19)$$

Therefore, there exists a positive constant C_3 depending on n and $\|v\|$ such that

$$\sum_{\mathbf{p} \in \Gamma_2} |v_{\mathbf{q}-\mathbf{p}}| |u_{\mathbf{p}}| \leq C_3 |\mathbf{q}|^{-\alpha+1}. \quad (3.20)$$

Combining Eqs. (3.12), (3.16) and (3.20), one obtains that

$$|u_{\mathbf{q}}| \leq 4|\mathbf{q}|^{-2} \left(\sum_{\mathbf{p} \in \Gamma_1} |v_{\mathbf{q}-\mathbf{p}}| |u_{\mathbf{p}}| + \sum_{\mathbf{p} \in \Gamma_2} |v_{\mathbf{q}-\mathbf{p}}| |u_{\mathbf{p}}| \right) \leq 4C_1 |\mathbf{q}|^{n-m-2} + 4C_3 |\mathbf{q}|^{-\alpha-1}. \quad (3.21)$$

Because $|u_{\mathbf{q}}| \leq C_\alpha |\mathbf{q}|^{-\alpha}$ holds, one obtains that $-\alpha \geq n-m-2$, which ends the proof. \square

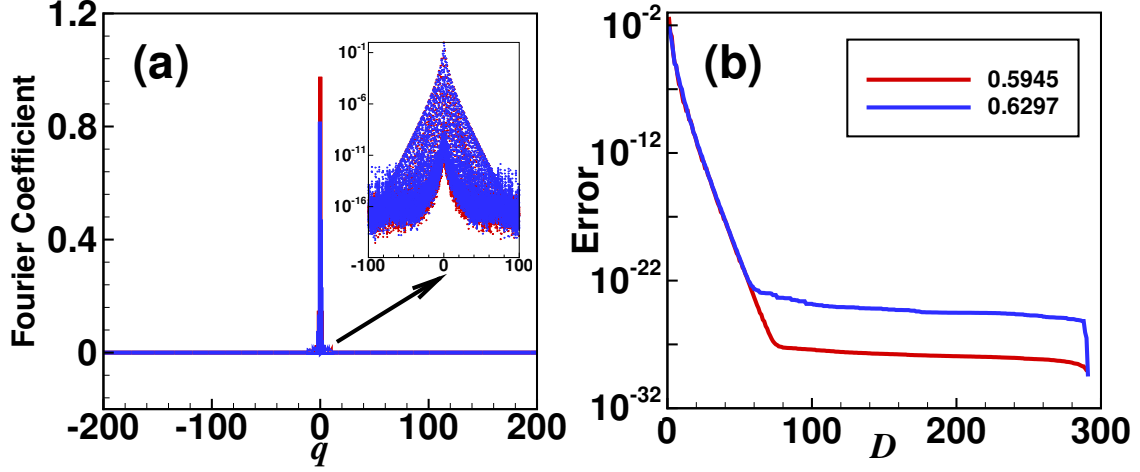


FIGURE 3.1. The generalized Fourier coefficient modulus of eigenfunctions for the 1D quasiperiodic potential. (a) The generalized Fourier coefficient modulus of eigenfunctions as function of q . (b) The error $\text{Err}(D)$ as function of D for spectrum 0.5945 and 0.6297. In both panels, $E_0 = 1$ and $N = 180$.

We employ a 1D quasiperiodic problem of (3.1) as an example to validate the theoretical result of Theorem 3.2. Let $v(z) = E_0/(1 + (\cos(z) + \cos(\sqrt{5}z))^2)$ and the projection matrix $\mathbf{P} = [\sqrt{5} \ 1]$. The PM is employed to solve this problem and depict the generalized Fourier coefficients of eigenfunctions in the raised frequency domain. As shown in Figure 3.1 (a), whether it is the eigenfunction corresponding to spectrum 0.5945 (the red line, the smallest spectrum) or the eigenfunction corresponding to spectrum 0.6297 (the blue line), their generalized Fourier coefficients both decay exponentially. We adopt the RPM to solve the same problem. In order to quantify the truncation error between the PM and RPM, we define

$$\text{Err}(D) = \sum_{|\mathbf{k}| > D, \mathbf{k} \in \Omega} |U_{\mathbf{k}}|^2. \quad (3.22)$$

Figure 3.1 (b) depict the exponential decay of $\text{Err}(D)$ with respect to D . For $D \approx 30$, the method has the machine precision and the reduction error becomes negligible, which accounts for more than 80% reduction of the DOF in the eigenvalue solver.

3.2. Numerical scheme. For the PM method, the Fourier approximation space of the numerical solution is given by $\mathbb{D} = \text{span}\{e^{i\langle \mathbf{k}, \mathbf{x} \rangle}, \mathbf{k} \in \Omega\}$ with the index set Ω given by

$$\Omega = \{\mathbf{k} \in \mathbb{Z}^n \mid \|\mathbf{k}\|_{\infty} \leq N\}. \quad (3.23)$$

As can be observed in Theorem 3.2, given some mild restrictions on the regularity of quasiperiodic potential function $v(\mathbf{z})$ and its parent function $V(\mathbf{x})$, the index set Ω of Fourier expansion can be reduced to

$$\Omega_R = \{\mathbf{k} \in \mathbb{Z}^n \mid \|\mathbf{P}\mathbf{k}\|_{\infty} \leq D, \|\mathbf{k}\|_{\infty} \leq N\} \quad (3.24)$$

without sacrificing the accuracy of the approximation. Here, parameter $D < N$ is a prescribed truncation constant. The RPM for the quasiperiodic problem (3.1) reads: find non-trivial $U_D^N \in \mathbb{D}_R = \text{span}\{e^{i\langle \mathbf{k}, \mathbf{x} \rangle}, \mathbf{k} \in \Omega_R\}$ and $E \in \mathbb{R}$ such that

$$\frac{1}{2}(\varphi(\nabla)U_D^N, \varphi(\nabla)W) + (G_D^N, W) = E(U_D^N, W), \quad W \in \mathbb{D}_R, \quad (3.25)$$

where $G_D^N = VU_D^N$ and

$$\varphi(\nabla) = \left(\sum_{i=1}^d P_{i1} \frac{\partial}{\partial x_1}, \dots, \sum_{i=1}^d P_{in} \frac{\partial}{\partial x_n} \right). \quad (3.26)$$

In what follows, we first give a rigorous estimate of the truncation error of the reduced space \mathbb{D}_R for quasiperiodic functions. For a quasiperiodic function f , the operators \mathcal{P} and \mathcal{Q} denote the partial sums

$$\mathcal{P}f = \sum_{\mathbf{q} \in \phi(\Omega)} f_{\mathbf{q}} e^{i\langle \mathbf{q}, \mathbf{z} \rangle} = \sum_{\mathbf{k} \in \Omega} F_{\mathbf{k}} e^{i\langle \mathbf{k}, \mathbf{x} \rangle}, \quad (3.27)$$

and

$$\mathcal{Q}f = \sum_{\mathbf{q} \in \phi(\Omega_R)} f_{\mathbf{q}} e^{i\langle \mathbf{q}, \mathbf{z} \rangle} = \sum_{\mathbf{k} \in \Omega_R} F_{\mathbf{k}} e^{i\langle \mathbf{k}, \mathbf{x} \rangle}, \quad (3.28)$$

where Ω and Ω_R are defined in Eqs. (3.23) and (3.24). In order to obtain the bound of the truncation error, one needs the following lemma (see [35]).

Lemma 3.1. *For any quasiperiodic function f with its parent function $F \in H_{\text{per}}^m([0, 2\pi]^n)$, $m \in \mathbb{Z}^+$, and $0 \leq \mu \leq m$, the following estimate for $\mathcal{P}f$ holds*

$$\|\mathcal{P}f - F\|_{\mu, \text{per}} \leq N^{\mu-m} |F|_{m, \text{per}}. \quad (3.29)$$

In addition, if $F \in H_{\text{per}}^\nu([0, 2\pi]^n)$ with $\nu > n/2$, there exists a constant C depending on ν such that

$$\|\mathcal{P}f - F\|_{\infty, \text{per}} \leq CN^{n/2-\nu} |F|_{\nu, \text{per}}. \quad (3.30)$$

The truncation error under different norms of operator \mathcal{Q} is bounded, as shown in Theorem 3.3.

Theorem 3.3. *Suppose that u is a quasiperiodic function. Let U be the parent function of u . If $U \in H_{\text{per}}^m([0, 2\pi]^n)$, $u \in H_{\text{qp}}^{m'}(\mathbb{R}^d)$ with $m, m' \in \mathbb{Z}^+$ and $0 \leq \mu < m \leq m'$, there exist constants C_1 and C_2 depending on $\|\mathbf{P}\|$ and μ such that*

$$\|\mathcal{Q}u - U\|_{\mu, \text{qp}} \leq C_1 N^{\mu-m} |U|_{m, \text{per}} + C_2 D^{\mu-m'} |u|_{m', \text{qp}}. \quad (3.31)$$

If $U \in H_{\text{per}}^\nu([0, 2\pi]^n)$, $u \in H_{\text{qp}}^\eta(\mathbb{R}^d)$ with $n/2 < \nu \leq \eta$, there exist constants C_3 and C_4 depending on λ, d, ν and η such that

$$\|\mathcal{Q}u - U\|_{\infty, \text{qp}} \leq C_3 N^{n/2-\nu} |U|_{\nu, \text{per}} + C_4 D^{n/2-\eta} |u|_{\eta, \text{qp}}. \quad (3.32)$$

Proof. By Lemma 3.1, if $U \in H_{\text{per}}^m([0, 2\pi]^n)$ with $m \in \mathbb{Z}^+$ and $0 \leq \mu \leq m$, one has

$$\|\mathcal{P}u - U\|_{\mu} \leq N^{\mu-m} |U|_{m, \text{per}}. \quad (3.33)$$

In addition, if $U \in H_{\text{per}}^\nu([0, 2\pi]^n)$ with $\nu > n/2$, there exists a constant C depending on ν satisfying

$$\|\mathcal{P}u - U\|_{\infty} \leq CN^{n/2-\nu} |U|_{\nu, \text{per}}. \quad (3.34)$$

By a direct decomposition $\mathcal{Q}u - u = (\mathcal{Q}u - \mathcal{P}u) + (\mathcal{P}u - U)$ and the triangle inequality, one has

$$\|\mathcal{Q}u - U\|_{\mu, \text{qp}} \leq \|\mathcal{Q}u - \mathcal{P}u\|_{\mu, \text{qp}} + \|\mathcal{P}u - U\|_{\mu, \text{qp}}, \quad (3.35)$$

$$\|\mathcal{Q}u - U\|_{\infty, \text{qp}} \leq \|\mathcal{Q}u - \mathcal{P}u\|_{\infty, \text{qp}} + \|\mathcal{P}u - U\|_{\infty, \text{qp}}. \quad (3.36)$$

Firstly consider the μ -norm case. For any $\mathbf{k} \in \Omega/\Omega_R$, $\|\mathbf{P}\mathbf{k}\|_{\infty} > D$ holds, so that

$$\|\mathcal{Q}u - \mathcal{P}u\|_{\mu, \text{qp}}^2 \leq D^{-2m'+2\mu} \sum_{\mathbf{q} \in \phi(\Omega/\Omega_R)} (1 + |\mathbf{q}|^{2\mu}) |u_{\mathbf{q}}|^2 |\mathbf{q}|^{2m'-2\mu} \lesssim D^{-2m'+2\mu} |u|_{m', \text{qp}}^2, \quad (3.37)$$

where $A \lesssim B$ denotes that A is less than or similar to B . Then by Lemma 3.1, if $U \in H_{\text{per}}^m([0, 2\pi]^n)$ with $m \in \mathbb{Z}^+$ and $0 \leq \mu \leq m$, one has

$$\|\mathcal{P}u - U\|_{\mu, \text{per}} \leq N^{\mu-m} |U|_{m, \text{per}}. \quad (3.38)$$

Then by the definition of the Sobolev spaces H_{per}^μ and H_{qp}^μ , one has

$$\|\mathcal{P}u - U\|_{\mu, \text{qp}} \leq \|\mathbf{P}\|^\mu \|\mathcal{P}u - U\|_{\mu, \text{per}}. \quad (3.39)$$

Combining Eqs. (3.37) and (3.39), the μ -norm case is proved.

On the other hand, one can use the Cauchy-Schwarz inequality to obtain

$$\|\mathcal{Q}u - \mathcal{P}u\|_{\infty, \text{qp}} \leq \sum_{\mathbf{q} \in \phi(\Omega/\Omega_R)} |u_{\mathbf{q}}| \leq \left(\sum_{\mathbf{q} \in \phi(\Omega/\Omega_R)} |\mathbf{q}|^{-2\eta} \right)^{1/2} \left(\sum_{\mathbf{q} \in \phi(\Omega/\Omega_R)} |\mathbf{q}|^{2\eta} |u_{\mathbf{q}}|^2 \right)^{1/2}. \quad (3.40)$$

For $\eta > n/2$,

$$\sum_{\mathbf{q} \in \phi(\Omega/\Omega_R)} |\mathbf{q}|^{-2\eta} = \sum_{\mathbf{k} \in \Omega/\Omega_R} |\mathbf{P}\mathbf{k}|^{-2\eta} \lesssim N^{n-d} \int_{|\mathbf{z}| \geq D} |\mathbf{z}|^{-2\eta} d\mathbf{z} = \frac{2^{2\eta-1}\pi}{2\eta-d} \lambda^{n-d} D^{n-2\eta}, \quad (3.41)$$

where C_0 is a positive constant depending on η and d . Hence by Eqs. (3.40) and (3.41), there exists a positive constant C_4 depending on λ, d and η such that

$$\|\mathcal{Q}u - \mathcal{P}u\|_{\infty, \text{qp}} \leq C_4 D^{n/2-\eta} |u|_{\eta, \text{qp}}. \quad (3.42)$$

By Lemma 3.1, one has

$$\|\mathcal{P}u - U\|_{\infty, \text{qp}} \leq C_3 N^{n/2-\nu} |U|_{\nu, \text{per}}, \quad (3.43)$$

where C_3 is a positive constant depending on ν . Then combining Eqs. (3.42) and (3.43), the infinite norm case is proved. \square

Remark 3.1. If the parent function $F(\mathbf{x}) \in H_{\text{per}}^m$, one can use Theorem 2.1 to obtain $f(\mathbf{z}) \in H_{\text{qp}}^m$. This is because

$$\|f(\mathbf{z})\|_{m, \text{qp}}^2 = \sum_{\mathbf{q} \in \mathbb{Z}[\text{col}(\mathbf{P})]} (1 + \|\mathbf{q}\|_2^{2m}) |f_{\mathbf{q}}|^2 = \sum_{\mathbf{k} \in \mathbb{Z}^n} (1 + \|\mathbf{P}\mathbf{k}\|_2^{2m}) |F_{\mathbf{k}}|^2 \leq C \|F(\mathbf{x})\|_{m, \text{qp}}, \quad (3.44)$$

where C is a positive constant depending on $\|\mathbf{P}\|$. Hence $m \leq m'$ and $\nu \leq \eta$ always hold, and the error decay rate of D is faster than that of N . This shows the feasibility of a secondary truncation along the direction of $\mathbf{P}\mathbf{k}$. This also implies that, if u and U have sufficiently good regularity, the truncation error can achieve exponential decay with respect to both N and D .

3.3. Solution Algorithm. In this part, we propose the detailed scheme of the RPM under the weak form Eq. (3.25) with the similar spatial notations in [36]. For the space domain $[0, 2\pi]^n$, consider the uniform length $h = 2\pi/N$ in each direction for an even positive integer N . Define $T_h = \{x = mh, m = 0, 1, \dots, N-1\}^n$. For any $U(\mathbf{x}) \in H_{\text{per}}^s([0, 2\pi]^n)$, define I_N as the trigonometric interpolation operator [35],

$$(I_N U)(\mathbf{x}) = \sum_{\mathbf{k} \in \Omega_R} \tilde{U}_{\mathbf{k}} e^{i\langle \mathbf{k}, \mathbf{x} \rangle}, \quad (3.45)$$

where the pseudo-spectral coefficients $\tilde{U}_{\mathbf{k}}$ are determined such that $(I_N U)(\mathbf{x}) = U(\mathbf{x}_h)$ hold for all $\mathbf{x}_h \in T_h$. The Fourier pseudo-spectral first and second order derivatives of $(I_N U)(\mathbf{x})$ along the x_1 direction are given by

$$\mathcal{D}_1(I_N U) = \sum_{\mathbf{k} \in \Omega_R} i k_1 \tilde{U}_{\mathbf{k}} e^{i\langle \mathbf{k}, \mathbf{x} \rangle}, \quad \mathcal{D}_1^2(I_N U) = - \sum_{\mathbf{k} \in \Omega_R} k_1^2 \tilde{U}_{\mathbf{k}} e^{i\langle \mathbf{k}, \mathbf{x} \rangle}. \quad (3.46)$$

The differentiation operators of other directions can be defined in a similar form. In turn, we can define the discrete higher-dimensional Laplacian in the point-wise sense by

$$\varphi(\Delta)(I_N U) = \sum_{\mathbf{k} \in \Omega_R} \tilde{U}_{\mathbf{k}} \text{tr}(\mathbf{P}\mathbf{H}_{\mathbf{x}}\mathbf{P}^\top) e^{i\langle \mathbf{k}, \mathbf{x} \rangle}, \quad (3.47)$$

where $\mathbf{H}_{\mathbf{x}}$ is the Hessian matrix under \mathbf{x} . By the properties of the orthonormal basis, it leads to a system of equations for each frequency mode $\tilde{U}_{\mathbf{k}}, \mathbf{k} \in \Omega_R$ by the properties of the orthonormal basis,

$$E \tilde{U}_{\mathbf{k}} = \frac{1}{2} \text{tr}(\mathbf{P}\mathbf{k}\mathbf{k}^\top \mathbf{P}^\top) \tilde{U}_{\mathbf{k}} + \sum_{\mathbf{m} \in \Omega_R} \tilde{V}_{\mathbf{k}-\mathbf{m}} \tilde{U}_{\mathbf{m}}. \quad (3.48)$$

One denotes that $\hat{\mathbf{U}}$ is an $|\Omega_R| \times 1$ column vector with its components being the Fourier coefficients $U_{\mathbf{k}}$, and the discrete eigenvalue problem Eq. (3.48) can be rewritten into a matrix eigenvalue problem $\mathbf{H}\hat{\mathbf{U}} = E\hat{\mathbf{U}}$. In real computations, due to the large size of the dense matrix \mathbf{H} , it is not practical to store its elements and the eigenvalue problem is to be solved in a matrix-free manner. That is, for matrix \mathbf{H} , one defines its matrix-vector product function

$$\mathbf{H}\mathbf{f} = \hat{\mathbf{D}}\mathbf{f} + \text{FFT}(V(\mathbf{x}) \cdot \text{IFFT}(\mathbf{f})), \quad (3.49)$$

where $\text{FFT}(\cdot)$ and $\text{IFFT}(\cdot)$ denote the n -dimensional fast Fourier transform (FFT) and inverse fast Fourier transform (IFFT). Here $\hat{\mathbf{D}}$ is a diagonal matrix such that for $\hat{\mathbf{U}}_m = \tilde{U}_{\mathbf{k}}$, the m th diagonal element of $\hat{\mathbf{D}}$ is

$$\hat{D}_{mm} = \frac{1}{2} \text{tr}(\mathbf{P}\mathbf{k}\mathbf{k}^\top \mathbf{P}^\top). \quad (3.50)$$

Since only the operation $\mathbf{H}\mathbf{f}$ is invoked during the generation of basis vectors in the Krylov subspace, there is no need to store the dense matrix \mathbf{H} itself, thus reducing the storage cost from $O(|\Omega_R|^2)$ to $O(|\Omega_R|)$. Then the eigenvalue problem (3.48) can be solved via the Krylov subspace iterative method in a matrix-free manner [37, 38]. When computing $\text{FFT}(V(\mathbf{x}) \cdot \text{IFFT}(\mathbf{f}))$, it is advisable to zero-fill the coefficients of \mathbf{f} removed by the RPM, thereby enabling the use of the IFFT. One multiplies $\text{IFFT}(\mathbf{f})$ by $V(\mathbf{x})$ in the physical space and then applies the FFT. After the FFT step, one reduces the coefficients in Ω/Ω_R again. Hence \mathbf{H} can still be considered as an $|\Omega_R| \times |\Omega_R|$ matrix. To solve the eigenvalues of \mathbf{H} by the Krylov subspace method, one takes a random starting vector $\mathbf{b} \in \mathbb{R}^{|\Omega_R| \times 1}$, and generates the Krylov subspace $K_M = \text{span}\{\mathbf{b}, \mathbf{H}\mathbf{b}, \dots, \mathbf{H}^{M-1}\mathbf{b}\}$. The orthonormal basis $\mathbf{Q}_M = (\mathbf{q}_1, \mathbf{q}_2, \dots, \mathbf{q}_M)$ of K_M can be generated by the implicitly restarted Arnoldi method [39]. One can determine the Hessenberg matrix $\mathbf{H}_M = \mathbf{Q}_M^\top \mathbf{H} \mathbf{Q}_M = \mathbf{Q}_M^\top (\mathbf{H}\mathbf{q}_1, \mathbf{H}\mathbf{q}_2, \dots, \mathbf{H}\mathbf{q}_M)$ and solve its eigenpairs $\{(E_m, u_m)\}_{m=1}^M$ of \mathbf{H}_M by the QR algorithm. Detailed procedures of the RPM are summarized in Algorithm 1.

Algorithm 1 The reduced projection method (RPM)

Input: d -dimensional quasiperiodic potential v , projection matrix \mathbf{P} , and parameter N , D , M , δ and ϵ

Output: Eigenpairs $\{(E_m, u_m)\}$

- 1: Compute the potential V in higher dimensional space by using \mathbf{P}
 - 2: Determine the index sets Ω_R and Ω of basis space by Eqs. (3.24) and (3.23) and take random starting vector $\mathbf{b} \in \mathbb{R}^{1 \times |\Omega_R|}$
 - 3: Expand \mathbf{b} to $\mathbf{b}' \in \mathbb{R}^{1 \times |\Omega|}$ by filling 0, compute $\text{FFT}(V(\mathbf{x}) \cdot \text{IFFT}(\mathbf{b}'))$ and remove the elements at the zero-filled positions
 - 4: Generate the matrix-vector product $\mathbf{H}\mathbf{b}$ by Eq. (3.49)
 - 5: Repeat steps 3 – 4 to calculate $\mathbf{H}^2\mathbf{b}, \dots, \mathbf{H}^{M-1}\mathbf{b}$ and generate the Krylov subspace K_M and its orthonormal basis \mathbf{Q}_M
 - 6: Determine Hessenberg matrix \mathbf{H}_M and compute its eigenpairs $\{(E_m, u_m)\}_{m=1}^M$ of \mathbf{H}_M
 - 7: Compute $U_N(\mathbf{x})$ by u_m and project the eigenfunctions $U_N(\mathbf{x})$ back into the d -dimensional space
-

By the RPM, the DOF and the complexity of the eigenvalue solver are significantly reduced. Specifically, the DOF of the eigenvalue solver for approximating a d dimensional quasiperiodic system with a $d \times n$ projection matrix using the PM is reduced from $O(N^n)$ to $O(N^{n-d}D^d)$. Correspondingly, the computational complexity of the proposed algorithm for solving the first k eigenpairs using the Krylov subspace method decreases from $O(kN^{2n})$ to $O(kN^{2(n-d)}D^{2d})$ [40, 41]. It is remarked that the zero-fill operation for the FFT leads to $O(N^n \log N)$ complexity. This complexity is usually much smaller than the $O(N^{2(n-d)}D^{2d})$ scaling, and the FFT calculation is only a small portion in the eigenvalue solver. Due to the fast decay of the generalized Fourier coefficients along $\mathbf{P}\mathbf{k}$, the RPM can thus obtain reliable numerical results with much fewer DOFs of the eigenvalue solver, thereby mitigating the curse of dimensions, especially for high-dimensional problems.

In the next part, we will give a rigorous error estimate of the RPM for quasiperiodic eigenvalue problems Eq. (3.1). Let $K : X \rightarrow X$ denote a compact operator. The space X has the inner product (\cdot, \cdot) and its associated norm $\|\cdot\|$. S_N is a subspace of X and the approximate operator K_N is from S_N to S_N . We define the two errors as

$$\epsilon_N = \epsilon_N(E) = \sup_{u \in M(E)} \inf_{\chi \in S_N} \|u - \chi\|, \quad \epsilon_N^* = \epsilon_N^*(E) = \sup_{v \in M^*(E)} \inf_{\chi \in S_N} \|v - \chi\|,$$

where $M(E)$ is the set of all normal eigenvectors of K corresponding to the eigenvalue E with the corresponding algebraic multiplicity being m . Here K^* is the dual operator of K and $M^*(E)$ is the set of all normal eigenvectors of K^* corresponding to approximating eigenvalues $\mathcal{E}_j, j = 1, \dots, m$. The following lemma is from [42].

Lemma 3.2. *Let E represent the eigenvalue of operator K , and $\mathcal{E}_j(N)$ denote the j th eigenvalue of the approximate operator K_N . There exists a constant C_0 such that*

$$|E - \mathcal{E}_j(N)| \leq C_0 (\epsilon_N \epsilon_N^*)^{1/\alpha}, j = 1, 2, \dots, m, \quad (3.51)$$

where α is the smallest nonnegative integral such that the null-spaces of $(E - K)^\alpha$ and $(E - K)^{\alpha+1}$ are equal.

Let $\mathcal{I}f$ represent the trigonometric interpolation associated with the RPM. Because of the use of the FFT and IFFT, the error analysis is quite different. The upper bound of the approximation under different norms of operator \mathcal{Q} to the eigenspace of Eq. (3.1) is given in Theorem 3.4.

Theorem 3.4. *Suppose that u is the solution of the quasiperiodic Schrödinger eigenvalue problem Eq. (3.1). Let U be the parent function of u . If $U \in H_{\text{per}}^m([0, 2\pi]^n), u \in H_{\text{qp}}^{m'}(\mathbb{R}^d)$ with $m, m' \in \mathbb{Z}^+$ and $0 \leq \mu < m \leq m'$, there exist constants C_1 and C_2 depending on $\|\mathbf{P}\|$ and μ such that*

$$\|\mathcal{I}u - U\|_{\mu, \text{qp}} \leq C_1 N^{\mu-m} |U|_{m, \text{per}} + C_2 D^{\mu-m'} |u|_{m', \text{qp}}. \quad (3.52)$$

If $U \in H_{\text{per}}^\nu([0, 2\pi]^n), u \in H_{\text{qp}}^\eta(\mathbb{R}^d)$ with $n/2 < \nu \leq \eta$, there exist constants C_3 and C_4 depending on λ, d, ν, n and η such that

$$\|\mathcal{I}u - U\|_{\infty, \text{qp}} \leq C_3 N^{n/2-\nu} |U|_{\nu, \text{per}} + C_4 D^{n/2-\eta} |u|_{\eta, \text{qp}}. \quad (3.53)$$

Proof. Because of the discrete orthogonality condition

$$(e^{i\langle \mathbf{k}_1, \mathbf{x} \rangle}, e^{i\langle \mathbf{k}_2, \mathbf{x} \rangle}) = \begin{cases} 1, & \mathbf{k}_1 = \mathbf{k}_2 + 2N\mathbf{m}, \mathbf{m} \in \mathbb{Z}^n, \\ 0, & \text{otherwise,} \end{cases} \quad (3.54)$$

one has

$$\mathcal{I}f = \mathcal{Q}f + \mathcal{R}f, \quad (3.55)$$

where

$$\mathcal{R}f = \sum_{\mathbf{k} \in \Omega_R} \left(\sum_{\mathbf{m} \in \mathbb{Z}^n \setminus \{\mathbf{0}\}} F_{\mathbf{k}+2N\mathbf{m}} \right) e^{i\langle \mathbf{k}, \mathbf{x} \rangle} \quad (3.56)$$

is the aliasing error. Then one has the decomposition $\mathcal{I}u - u = (\mathcal{Q}u - \mathcal{P}u) + (\mathcal{P}u - U) + \mathcal{R}u$. By the triangle inequality, one has

$$\|\mathcal{I}u - U\|_{\mu, \text{qp}} \leq \|\mathcal{Q}u - \mathcal{P}u\|_{\mu, \text{qp}} + \|\mathcal{P}u - U\|_{\mu, \text{qp}} + \|\mathcal{R}u\|_{\mu, \text{qp}}, \quad (3.57)$$

$$\|\mathcal{I}u - U\|_{\infty, \text{qp}} \leq \|\mathcal{Q}u - \mathcal{P}u\|_{\infty, \text{qp}} + \|\mathcal{P}u - U\|_{\infty, \text{qp}} + \|\mathcal{R}u\|_{\infty, \text{qp}}. \quad (3.58)$$

One can obtain that there exist constants C_1 and C_2 depending on μ , such that [43]

$$\|\mathcal{R}u\|_{\mu, \text{per}} \leq C_1 N^\mu \|\mathcal{R}u\|_{L^2} \leq C_2 N^{\mu-s} |U|_{s, \text{per}}. \quad (3.59)$$

Then

$$\|\mathcal{R}u\|_{\mu, \text{qp}} \leq \|\mathbf{P}\|^\mu \|\mathcal{R}u\|_{\mu, \text{per}} \quad (3.60)$$

holds. In addition, applying the Cauchy-Schwarz inequality, there exists a constant C_3 depending on ν and n such that

$$\|\mathcal{R}u\|_{\infty, \text{per}} \leq \sum_{\mathbf{k} \in \Omega_R} \sum_{\mathbf{m} \in \mathbb{Z}^n \setminus \{\mathbf{0}\}} |U_{\mathbf{k}+2N\mathbf{m}}| \leq \sum_{\mathbf{k} \in \Omega^C} |U_{\mathbf{k}}| \leq C_3 N^{n/2-\nu} |U|_{\nu, \text{per}}. \quad (3.61)$$

By using Theorem 3.3, both cases are proved. \square

One has Corollary 3.1 for the error estimate of the RPM with space basis Ω_R by Lemma 3.2 and Theorem 3.4.

Corollary 3.1. *Let E represent the eigenvalue of the Schrödinger operator, and $\mathcal{E}_j(N, D)$ denote the j th corresponding eigenvalue of the RPM. The error of E is bounded under the μ -norm by*

$$|E - \mathcal{E}_j(N, D)| \leq (C_0 N^{\mu-m} |U|_{m, \text{per}} + C D^{\mu-m'} |u|_{m', \text{qp}})^{2/\alpha}, \quad (3.62)$$

where $0 \leq \mu < m \leq m'$, and under the infinite norm by

$$|E - \mathcal{E}_j(N, D)| \leq (C_0 N^{n/2-\eta} |U|_{\nu, \text{per}} + C D^{n/2-\eta} |u|_{\eta, \text{qp}})^{2/\alpha}, \quad (3.63)$$

where $n/2 < \mu \leq \eta$, and C and C_0 are constants.

Corollary 3.1 establishes a rigorous theoretical foundation for solving the quasiperiodic Schrödinger eigenvalue problem using the RPM. Although the dimension lift significantly enlarges the DOF, the distinctive properties of the Fourier coefficients enable the resolution of larger-scale problems with a noticeably reduced number of the DOF of the eigenvalue solver by the RPM.

4. NUMERICAL EXAMPLES

We present numerical results to demonstrate the effectiveness of the RPM. Specifically, we apply the algorithm to quasiperiodic Schrödinger eigenvalue problems for moiré lattices in 1D and 2D spaces and assess the quality of the resulting solutions, as well as the CPU time. A matrix-free preconditioned Krylov subspace method [44, 45, 46, 47] is employed which requires only the matrix-vector product to be stored at each iteration. In these examples, we compare the RPM with the PM, which shows the accuracy and efficiency of the RPM. The calculations presented in this section are executed using Matlab code on an Intel TM core with a clock rate of 2.50 GHz and 32 GB of memory.

4.1. 1D example. We first examine the performance of the RPM for the 1D case. To be specific, we adopt the potential function in Eq. (3.1) to be those for 1D moiré lattices [7], expressed by

$$v_1(z) = \frac{E_0}{[\cos(2 \cos(\theta/2)z) + \cos(2 \sin(\theta/2)z)]^2 + 1}, \quad (4.1)$$

with $\theta = \pi/6$. The projection matrix is $\mathbf{P} = [2 \cos(\theta/2), 2 \sin(\theta/2)]$.

We take $E_0 = 1$. We fix the number of Fourier expansions to be $N = 180$ and depict in Figure 4.1 the DOF of the eigenvalue solver and condition numbers of \mathbf{H} in Eq. (3.49) against the truncation parameter D . It can be observed clearly that both the DOF and condition numbers decrease rapidly with the decrease of D . For comparison, the DOF of the original PM is $N^2 = 32400$, much bigger than that of the RPM for small D . Thus, a small D not only leads to a matrix eigenvalue system of much smaller size, but also reduces the number of iterations to converge. These observations highlight the potential of using the RPM to solve high-dimensional quasiperiodic eigenvalue problems.

To demonstrate the exceptional accuracy and rapid convergence of the RPM approach, we present error plots in Figure 4.2 for the potential function with $E_0 = 1$. The “exact” eigenvalues and eigenfunctions are determined using the numerical results obtained from the PM when $N = 300$. The error of eigenvalue, ε , is measured by the absolute error of the first eigenvalue. The error of the first normalized eigenfunction is also measured by the L^2 -norm in interval $[0, 1]$, which is denoted by δ . Fig. 4.2 illustrates the convergence with the increase of N for $D = 15, 20$ and 25 , and the convergence with the increase of D for $N = 20$ and 30 , characterized by both ε and δ . Panels (a,b) illustrate that both ε and δ exhibit an exponential

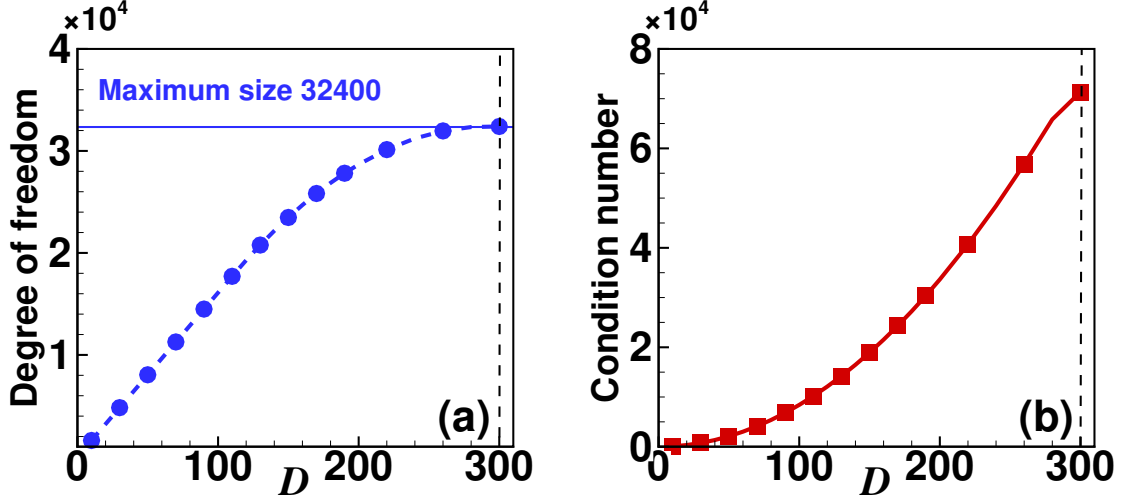


FIGURE 4.1. The DOF (a) and the condition number (b) as function of D using the RPM in one dimension with $N = 180$. Correspondingly, the DOF of the PM is $N^2 = 32400$.

decrease as N increases, eventually attaining a fixed value. It is notable that the magnitude of this fixed value diminishes with the increase of D . For relatively small values of N and D (e.g. $N = 30$ and $D = 20$), ϵ is already smaller than 10^{-10} and δ is smaller than 10^{-8} , demonstrating the high accuracy of the RPM. Panels (c,d) exhibit exponential decays with the increase of D , which is in agreement with the error analysis. When D is small ($D \leq 15$), the error curves of $N = 20$ and 30 almost overlap, indicating that the error mainly comes from the basis reduction. When D is large, the error curves of the two cases have a significant difference, indicating that the error is mainly caused by the PM part. Overall, one can observe that high accuracy of the results is remained in spite of a significant reduction in the number of bases.

In Table 4.1, we display the DOF in the RPM and the CPU time for the 1D system with $E_0 = 1$ for $N = 50, 100$ and 150 with D increasing from 10 to 50 . The DOF increases linearly with D . Theoretically, the RPM of 1D systems has complexity $O(D^2)$ for given N , and $O(N^2)$ for given D . Correspondingly, the complexity of the original PM is $O(N^4)$. Moreover, the condition number of the RPM is much smaller than the PM, as shown in Fig. 4.1. The results of the CPU time validate the complexity analysis. We have shown that a small D can achieve high accuracy. At $N = 50$, setting $D = 20$ has error as small as 10^{-10} . In this case, the CPU time for the RPM is 1.46 seconds, 11.6 times faster than that of the original PM. The reduction for large N is more significant. For $N = 150$, the speedup with $D = 20$ reaches 317.0 times. Correspondingly, with $N = 50, 100$ and 150 , the DOF of the original PM for $D = 20$ are 2.4, 4.8 and 7.2 times greater than those of the RPM, respectively. These results clearly demonstrate the attractive performance of the RPM.

Figure 4.3 depicts the error of the normalized first eigenfunction in interval $z \in [0, 1]$. We take $D = 25$ for $N = 20, 40$ and 60 , and calculate the absolute error for different $E_0 = 1, 2, 4$ and 8 where the “exact” eigenfunctions are generated by using the numerical results of the PM with $N = 300$. One can observe that the error converges with the increase of N . With the increase of E_0 , the error of the RPM increases. This is because E_0 describes the optical response strength in the photorefractive crystal [2]. For a large E_0 , the eigenfunction can become localized, leading to an obvious singularity. The results in panels (cd) illustrate that the RPM remains high accuracy with a small D with $N = 60$, demonstrating that the RPM is efficient for simulating challenging problems such as localization-delocalization transition in photonic moiré lattices.

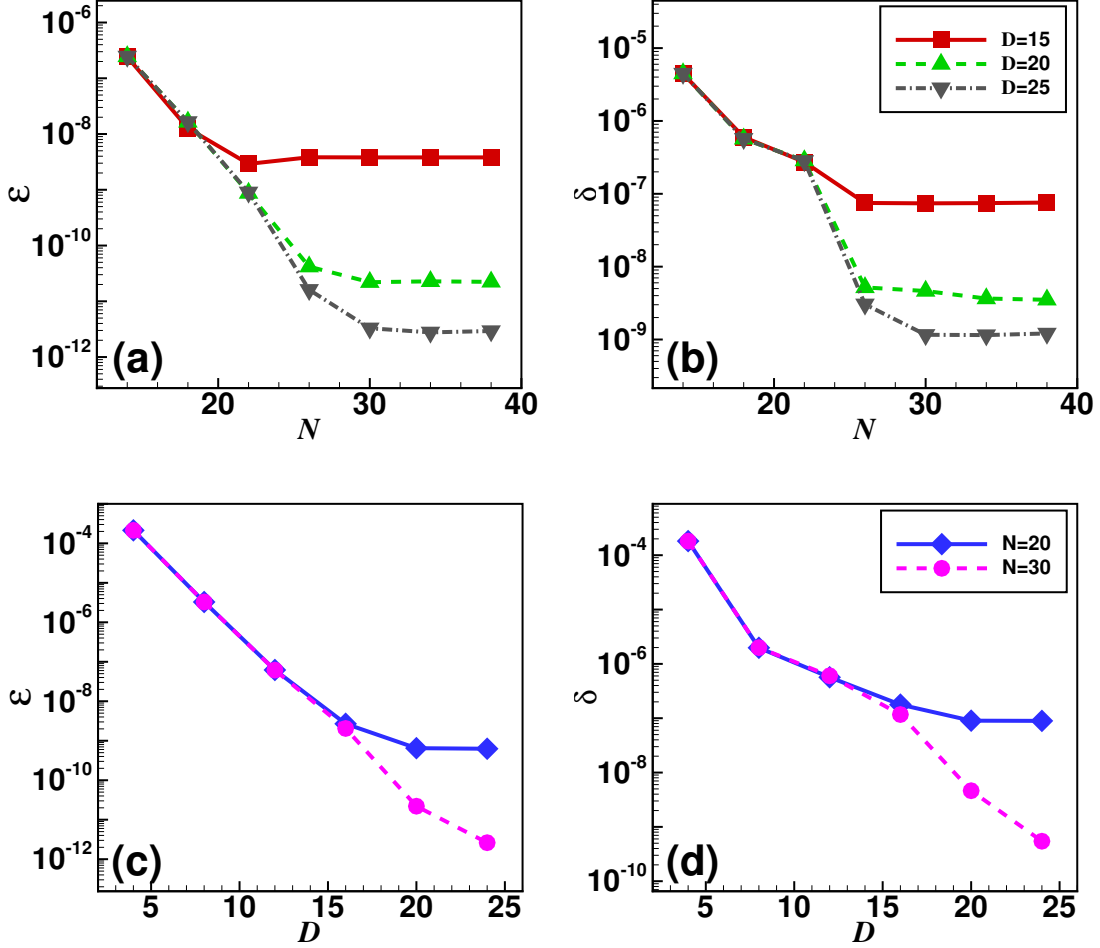


FIGURE 4.2. Absolute error of eigenvalues ε and the L^2 -error of the first eigenfunction δ . (a,b): Error as function of N for different D . (c,d): Error as function of D for different N .

4.2. 2D example. Consider a 2D example with the potential function taking

$$v_2(z_1, z_2) = \frac{E_0}{(\cos z_1 \cos z_2 + \cos(\sqrt{5}z_1) \cos(\sqrt{5}z_2))^2 + 1}. \quad (4.2)$$

This potential possesses the same structure as 2D moiré lattices [2, 7], making it applicable to simulations of photonic lattices. Correspondingly, the projection matrix is given by,

$$\mathbf{P} = \begin{bmatrix} 1 & 0 & \sqrt{5} & 0 \\ 0 & 1 & 0 & \sqrt{5} \end{bmatrix}. \quad (4.3)$$

We first calculate the generalized Fourier coefficients of eigenfunctions of the system. We set $E_0 = 1$ and $N = 30$. In Figure 4.4, we show the modulus of the coefficients for the 1st and 4th eigenfunctions in the \mathbf{q} space, calculated by the PM. The data are present with values of logarithms 10. One can observe the exponential decay of the generalized Fourier coefficients for both eigenfunctions. In each panel, there is only one peak in the origin of the \mathbf{q} space, and far from the origin the contributions of the Fourier modes are insignificant. Table 4.2 presents the error measured by $\text{Err}(D)$ in Eq. (3.22) of eigenfunctions

TABLE 4.1. The DOF and CPU time of the RPM for different N and D

	D	$N = 50$		$N = 100$		$N = 150$	
		DOF	CPU time (s)	DOF	CPU time (s)	DOF	CPU time (s)
PM	-	2500	17.010	10000	320.604	22500	3179.439
RPM	50	2373	9.382	5177	35.500	7766	123.172
	45	2236	8.389	4659	21.791	6990	85.054
	40	2048	5.690	4141	17.595	6210	61.924
	35	1811	4.433	3623	11.190	5434	42.748
	30	1552	3.110	3106	9.733	4658	30.751
	25	1295	2.266	2587	5.404	3881	18.599
	20	1034	1.460	2069	3.529	3106	10.029
	15	777	1.000	1551	2.456	2328	6.542
	10	517	0.452	1035	1.050	1552	2.800

corresponding to spectrum 0.4961 (the smallest one) and 0.4975 with the truncation constant D for $N = 30$. Again, one can observe rapid decays with respect to D for both cases. These results are similar to the 1D case and demonstrate that the approximation in the reduced space can be of high accuracy for the eigenproblem.

TABLE 4.2. Error of eigenfunctions as function of D in two dimensions

D	Err(D)		D	Err(D)	
	0.4961	0.4975		0.4961	0.4975
5	1.54E-05	2.19E-05	35	9.93E-15	1.58E-13
10	1.19E-07	1.16E-07	40	6.36E-16	7.36E-14
15	2.66E-09	2.50E-09	45	4.76E-17	3.40E-14
20	6.40E-11	7.30E-11	50	3.79E-18	1.52E-14
25	2.91E-12	3.20E-12	55	2.88E-19	2.68E-15
30	1.61E-13	3.71E-13	60	2.23E-20	1.73E-16

Figure 4.5 presents the DOF and condition number of the RPM as function of D with same setup: $E_0 = 1$ and $N = 30$. Again, both the DOF and condition number increase rapidly with the increase of D . In spite that $N = 30$ is not big, the DOF of the entire system in the raised 4D space, $N^4 = 810000$, is a very big number. From the results, we can see that the use of a small D can significantly reduce computational complexity, not only the size of the matrix eigenvalue problem, but also the iteration number in the solver of the implicitly restarted Arnoldi method.

We next study the accuracy and convergence of the RPM with $E_0 = 1$, and the results are presented in Figure 4.6. In the calculations, the “exact” eigenvalues and eigenfunctions are obtained from numerical results of the PM with $N = 32$. The errors are measured, where ε represents the absolute error of the first eigenvalue, and δ represents the error of the first eigenfunction using the L^2 norm in interval $[0, 1]^2$. Panels (a,b) illustrate the convergence of the numerical solution with the increase of N for truncation coefficient $D = 10, 20$ and 30 . Both ε and δ decay exponentially with increasing N , eventually converging to a fixed value which depends on D . Similar to the 1D case, small value of D results in high accurate results. For $D = 10$ (with a slightly bigger N), the RPM can achieve accuracy at the level of 10^{-5} in both the eigenvalue and eigenfunction calculation. Panels (c,d) displays the convergence with the increase of D for $N = 20$ and 28 . One can observe the exponential decays with D at the beginning, as expected from the previous error analysis. For small D , the error curves for $N = 20$ and 28 almost overlap, suggesting that the reduction of the basis space dominates the error. With a mediate D , the two curves in both

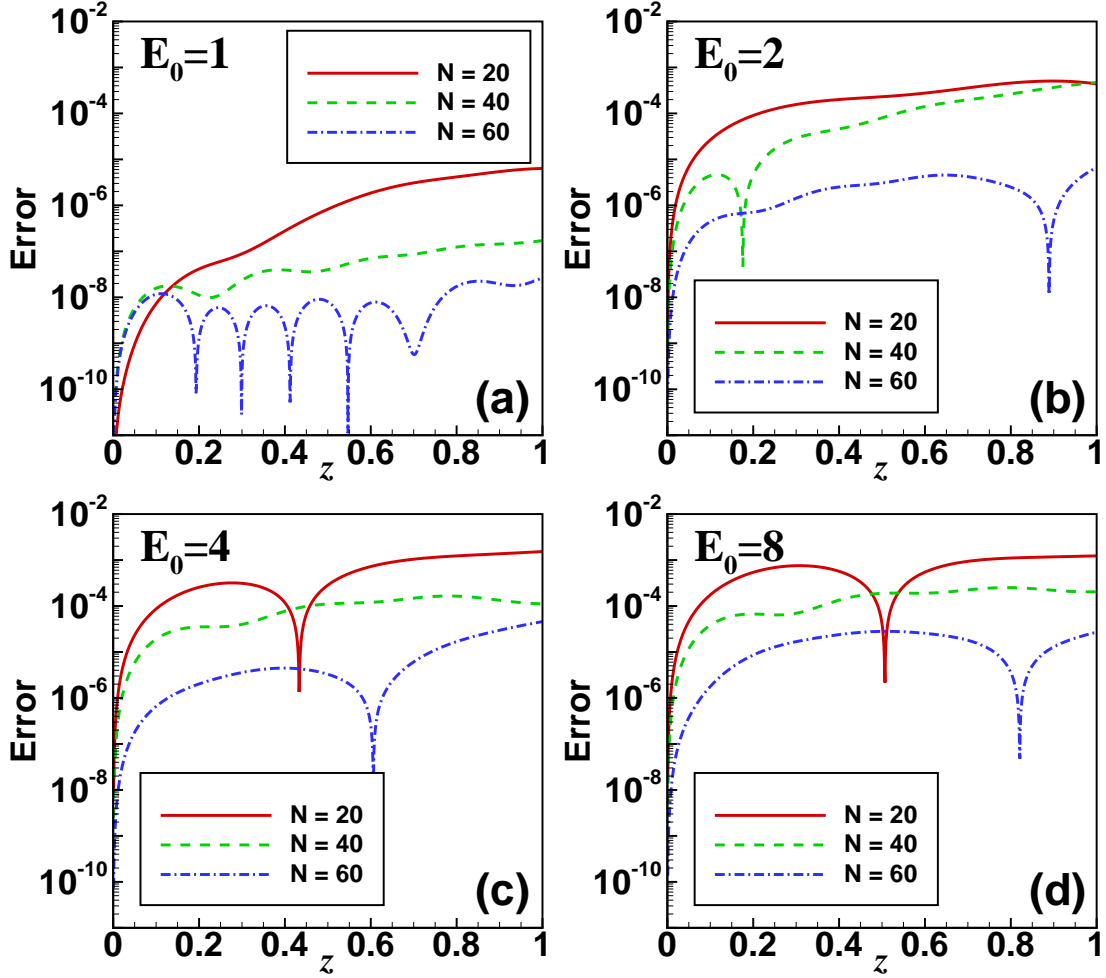


FIGURE 4.3. Error of the normalized first eigenfunctions obtained by the RPM in interval $[0, 1]$ for different E_0 . In each panel, $D = 25$ and three different N are calculated.

panels differ significantly, indicating that the error at this point mainly comes from the PM part. Overall, the accuracy with small D (e.g., $D = 10$) is good enough to provide accurate solutions. These findings demonstrate that high accuracy can be maintained by a significant reduction for basis functions.

We next conduct the study on the DOF and CPU time required for the RPM for the 2D system with $E_0 = 1$ for $N = 20, 24$ and 28 with D increasing from 10 to 30 , and the results are summarized in Table 4.3. The DOF exhibits a quadratic decrease with respect to D . Theoretically, the RPM of 2D systems has complexity $O(D^4)$ for given N , and $O(N^4)$ for given D , while the complexity of the original PM is $O(N^8)$. The numerical results of Table 4.3 are in agreement with these theoretical analysis. It also can be found that a small D is able to reach high accuracy. For $N = 20$, the use of $D = 10$ achieves an error level of 10^{-5} . In this case, the CPU time for the RPM is 148.50 seconds which is 15.8 times faster than that of the PM, and the DOF is 4.9 times smaller than that of the PM. The reduction for larger N will be more significant. When $N = 28$, the speedup with $D = 10$ becomes 73.8 times for the CPU time, and the reduction in the DOF is 9.7 times, comparing the RPM with the PM. One can see this speedup is even more larger than 1D problems by introducing the reduction technique in the PM.

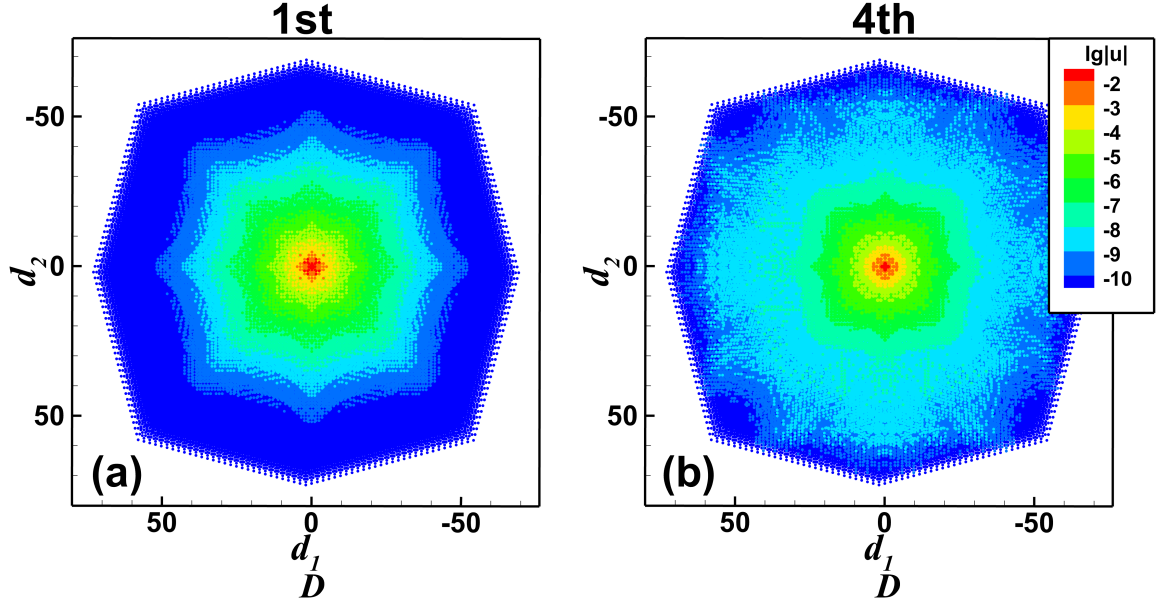


FIGURE 4.4. The generalized Fourier coefficients (modulus) of eigenfunctions in the q space for $E_0 = 1$ and $N = 30$. Results are present by logarithms with base 10.

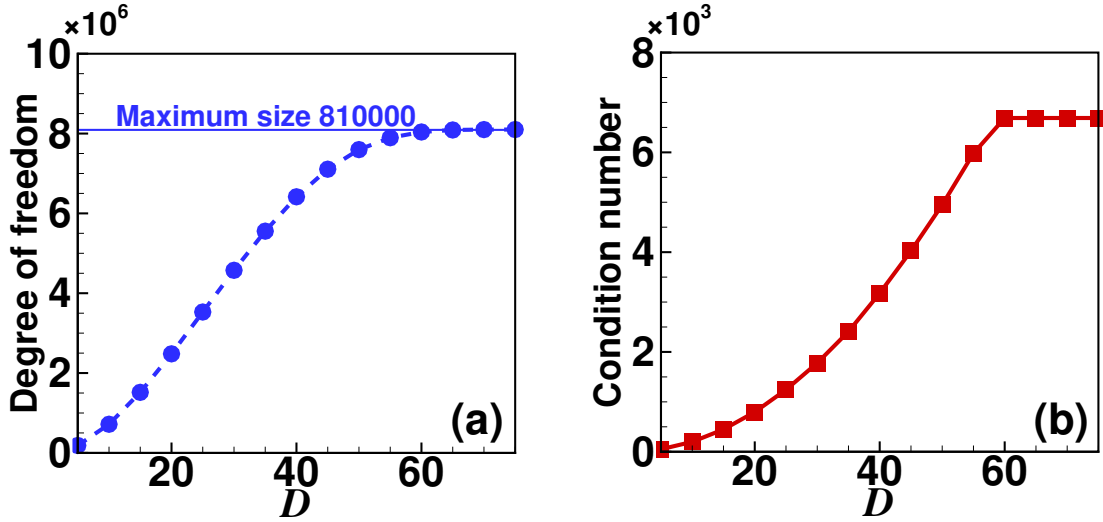


FIGURE 4.5. The DOF (a) and the change of condition number (b) with respect to D of the RPM in 2D. $N = 30$ and the maximum DOF is $N^4 = 810000$.

Finally, we investigate the performance of the RPM for varying E_0 . Figure 4.7 shows the profiles of the first eigenfunctions in 2D quasiperiodic systems for various E_0 and N . With the increase of E_0 , the eigenfunction becomes singular, leading to a localized eigenstate. This phenomenon is reminiscent of the localization-delocalization transition exhibited in experimental studies of 2D photonic moiré lattices [2]. The moiré lattices rely on flat-band structures for wave localization as opposed to the disordered media

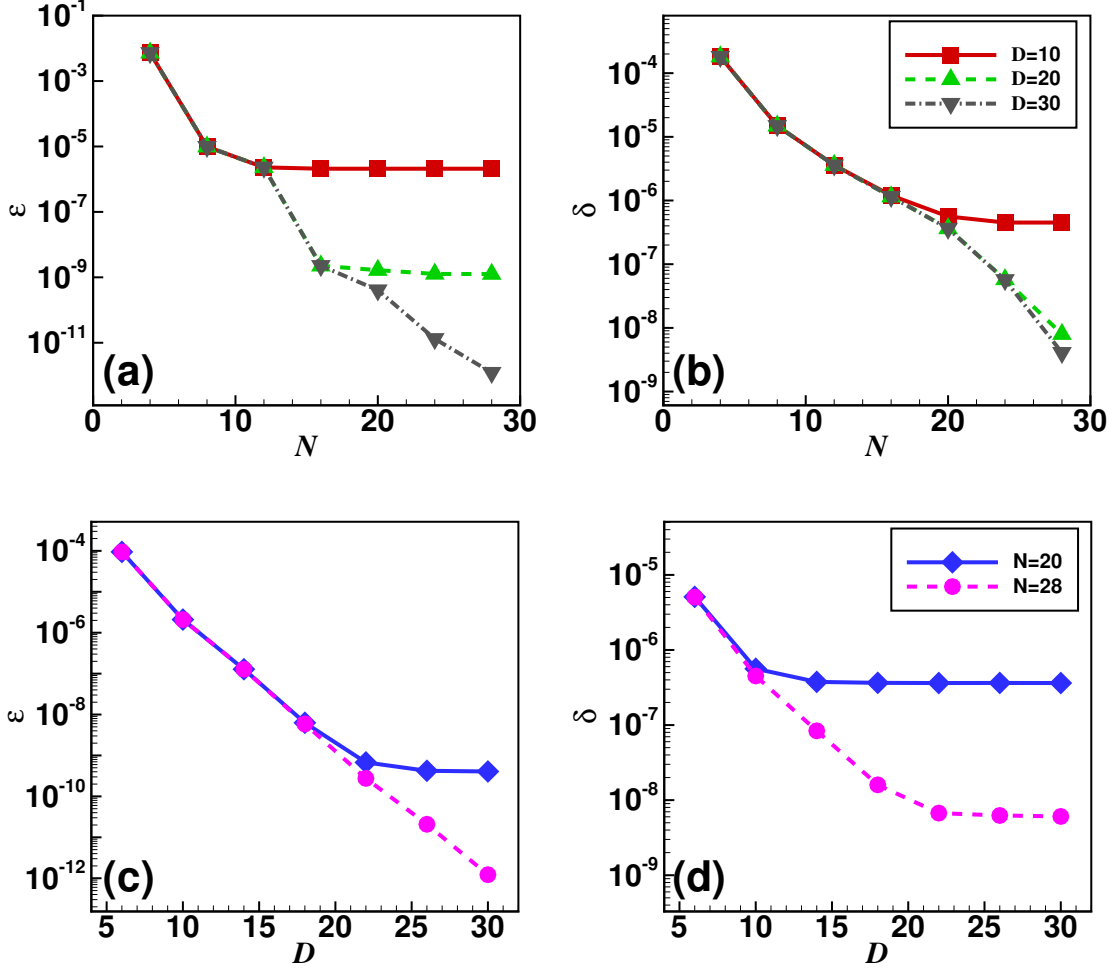


FIGURE 4.6. Errors of the first eigenvalue and eigenfunction. (a,b): Error as function of N for different D . (c,d): Error as function of D for different N .

used in other approaches based on light diffusion in photonic quasicrystals [48, 49]. The localization-delocalization transition of the eigenstates in 2D systems provide valuable insight into the exploration of quasicrystal structures. This transition process is displayed in Figure 4.7. The figure also illustrates that the results of different N are basically the same for the four different E_0 , indicating that the RPM converges fast for cases of both low and strong strength of optical response. Moreover, because of the lower DOF of the RPM, one can expect that more numerical nodes in each dimension can be applied to achieve higher accuracy of approximation.

5. CONCLUSIONS

We have proposed a reduced projection method (RPM) for accurate and fast calculations of eigenvalue problems for photonic quasicrystals. We show that the fast decay of the generalized Fourier coefficients for eigenfunctions of the quasiperiodic problems, justifying the efficiency of the RPM. The error bound of the approximation is provided, which demonstrates the high accuracy from theoretical point of view. Compared to the original PM, the reduced method requires much less memory and significantly speeds

TABLE 4.3. The DOF and CPU time of the RPM for different N and D in two dimensions

	D	$N = 20$		$N = 24$		$N = 28$	
		Size	CPU time (s)	Size	CPU time (s)	Size	CPU time (s)
PM	-	160000	2343.2	331776	10305	614656	32901
RPM	30	156816	2089.2	291600	6681.5	459684	15591
	28	152100	1927.7	273529	5760.1	421201	11562
	26	145161	1803.2	252004	4807.6	379456	9889.5
	24	135424	1552.9	227529	4318.9	335241	7631.6
	22	123201	1284.0	200704	3144.2	291600	6118.3
	20	108900	1057.3	173889	2362.0	247009	4035.2
	18	94249	786.30	145924	1895.6	202500	3363.2
	16	78400	650.76	117649	1409.2	160801	1832.3
	14	62001	424.71	90601	821.09	123904	1341.1
	12	46225	319.53	66564	493.80	91204	763.4
	10	32400	148.50	46656	304.35	63504	446.09

up the calculation, making it possible to calculate high-dimensional quasiperiodic eigenvalue problems. Numerical results in both 1D and 2D problems show the efficiency and accuracy of the algorithm, demonstrating attractive features for a broader applications for practical problems. The RPM is potentially useful to solve 3D or other problems rather than the Schrödinger system, which will be reported in our future work.

ACKNOWLEDGEMENT

Z. G. and Z. X. are supported by the National Natural Science Foundation of China (NNSFC)(grants No. 12325113 and 12071288), Science and Technology Commission of Shanghai Municipality (grant No. 21JC1403700), and the HPC center of Shanghai Jiao Tong University. Z. Y. is supported by the NNSFC (No. 12101399) and the Shanghai Sailing Program (No. 21YF1421000). The authors also thank Professor Huajie Chen from Beijing Normal University and Professor Kai Jiang from Xiangtan University for helpful discussions.

REFERENCES

- [1] F. Lei and C. Wang. Study on the properties of solitons in Moiré lattice. *Optik*, 219:165169, 2020.
- [2] P. Wang, Y. Zheng, X. Chen, C. Huang, Y.V. Kartashov, L. Torner, V.V. Konotop, and F. Ye. Localization and delocalization of light in photonic Moiré lattices. *Nature*, 577(7788):42–46, 2020.
- [3] Y. Cao, V. Fatemi, S. Fang, K. Watanabe, T. Taniguchi, E. Kaxiras, and P. Jarillo-Herrero. Unconventional superconductivity in magic-angle graphene superlattices. *Nature*, 556(7699):43–50, 2018.
- [4] L. Britnell, R.M. Ribeiro, A. Eckmann, R. Jalil, B.D. Belle, A. Mishchenko, Y. Kim, R.V. Gorbachev, T. Georgiou, and S.V. Morozov. Strong light-matter interactions in heterostructures of atomically thin films. *Science*, 340(6138):1311–1314, 2013.
- [5] M. Xu, T. Liang, M. Shi, and H. Chen. Graphene-like two-dimensional materials. *Chemical Reviews*, 113(5):3766–3798, 2013.
- [6] C. Huang, F. Ye, X. Chen, Y.V. Kartashov, V.V. Konotop, and L. Torner. Localization-delocalization wavepacket transition in Pythagorean aperiodic potentials. *Scientific Reports*, 6(1):1–8, 2016.
- [7] Z. Gao, Z. Xu, Z. Yang, and F. Ye. Pythagoras superposition principle for localized eigenstates of two-dimensional moiré lattices. *Physical Review A*, 108(8):013513, 2023.
- [8] X. Lu, P. Stepanov, W. Yang, M. Xie, M.A. Aamir, I. Das, C. Urgell, K. Watanabe, T. Taniguchi, G. Zhang, A. Bachtold, A. H. MacDonald, and D. K. Efetov. Superconductors, orbital magnets and correlated states in magic-angle bilayer graphene. *Nature*, 574(7780):653–657, 2019.
- [9] X. Zhang, Y. Peng, and D. Piao. Quasi-periodic solutions for the general semilinear duffing equations with asymmetric nonlinearity and oscillating potential. *Science China Mathematics*, 64:931–946, 2021.
- [10] R. Bistritzer and A.H. MacDonald. Moiré bands in twisted double-layer graphene. *Proceedings of the National Academy of Sciences*, 108(30):12233–12237, 2011.

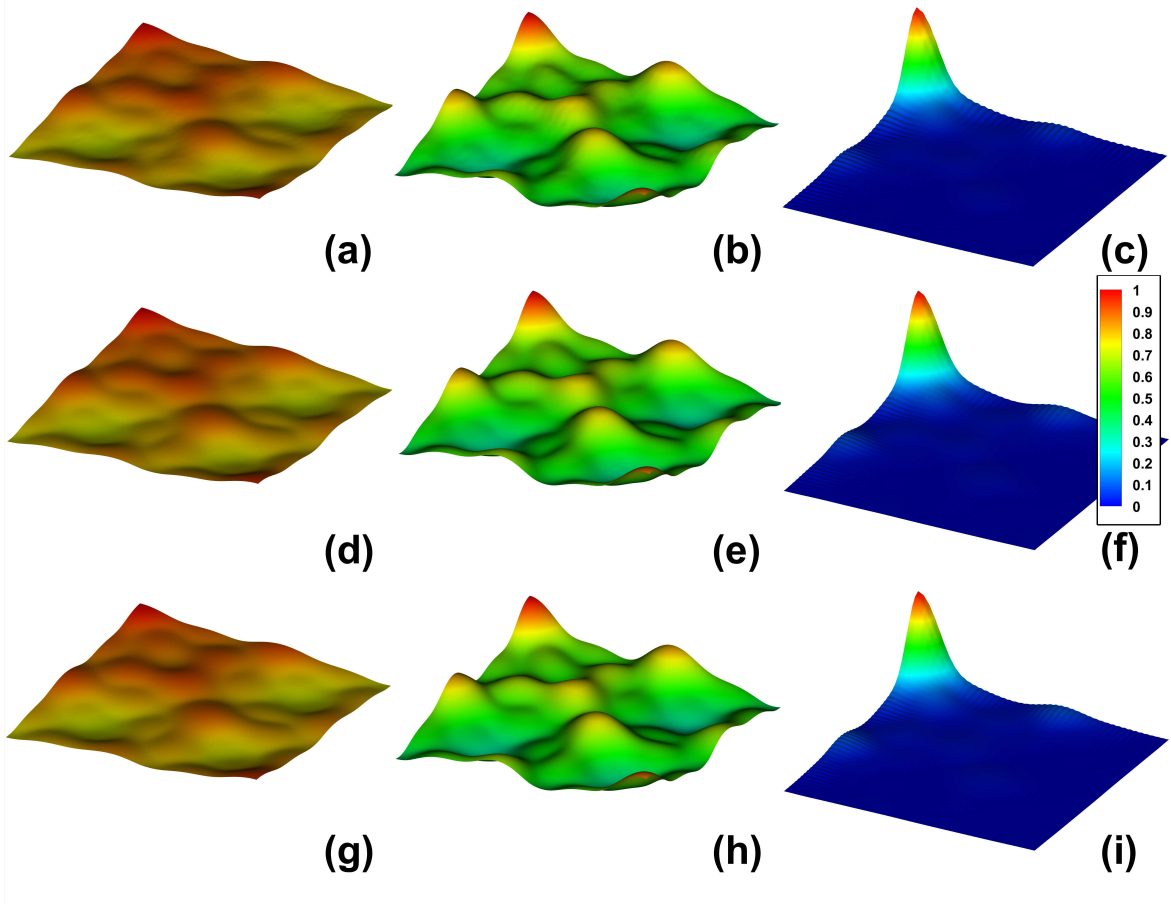


FIGURE 4.7. The normalized first eigenfunction $|u|$ in 2D under different E_0 and N . $D = 30$ is taken and the results in area $[0, 10]^2$. (a,b,c): $N = 24$, (d,e,f): $N = 26$ and (g,h,i): $N = 28$. (a,d,g): $E_0 = 0.25$, (b,e,h): $E_0 = 1$ and (c,f,i): $E_0 = 4$.

- [11] S. Carr, D. Massatt, S. Fang, P. Cazeaux, M. Luskin, and E. Kaxiras. Twistronics: Manipulating the electronic properties of two-dimensional layered structures through their twist angle. *Physical Review B*, 95(7):075420, 2017.
- [12] A. González-Tudela and I. Cirac. Cold atoms in twisted-bilayer optical potentials. *Physical Review A*, 100(5):053604, 2019.
- [13] L.J. O’Riordan, A. White, and T. Busch. Moiré superlattice structures in kicked Bose-Einstein condensates. *Physical Review A*, 93(2):023609, 2016.
- [14] G. Hu, A. Krasnok, Y. Mazor, C. Qiu, and A. Alù. Moiré hyperbolic metasurfaces. *Nano Letters*, 20(5):3217–3224, 2020.
- [15] K. Jiang, S. Li, and P. Zhang. Numerical analysis of computing quasiperiodic systems. *arXiv:2210.04384*.
- [16] Q. Fu, P. Wang, C. Huang, Y.V. Kartashov, L. Torner, V.V. Konotop, and F. Ye. Optical soliton formation controlled by angle twisting in photonic moiré lattices. *Nature Photonics*, 14(11):663–668, 2020.
- [17] Y.V. Kartashov, F. Ye, V.V. Konotop, and L. Torner. Multifrequency solitons in commensurate-incommensurate photonic moiré lattices. *Physical Review Letters*, 127(16):163902, 2021.
- [18] D. Kouznetsov, P. Van Dorpe, and N. Verellen. Sieve of eratosthenes for Bose-Einstein condensates in optical moiré lattices. *Physical Review A*, 105(2):L021304, 2022.
- [19] N.S. Salakhova, I.M. Fradkin, S.A. Dyakov, and N.A. Gippius. Fourier modal method for moiré lattices. *Physical Review B*, 104(8):085424, 2021.
- [20] H. Davenport and K. Mahler. Simultaneous Diophantine approximation. *Duke Mathematical Journal*, 13(1):105–111, 1946.

- [21] A.L. Goldman and R. Kelton. Quasicrystals and crystalline approximants. *Reviews of Modern Physics*, 65(1):213, 1993.
- [22] R. Lifshitz and D.M. Petrich. Theoretical model for Faraday waves with multiple-frequency forcing. *Physical Review Letters*, 79(7):1261, 1997.
- [23] A.W. Rodriguez, A.P. McCauley, Y. Avniel, and S.G. Johnson. Computation and visualization of photonic quasicrystal spectra via Bloch’s theorem. *Physical Review B*, 77(10):104201, 2008.
- [24] K. Jiang and P. Zhang. Numerical methods for quasicrystals. *Journal of Computational Physics*, 256:428–440, 2014.
- [25] K. Jiang and P. Zhang. Numerical mathematics of quasicrystals. In *Proceedings of the International Congress of Mathematicians: Rio de Janeiro 2018*, pages 3591–3609. World Scientific, 2018.
- [26] T. Wang, H. Chen, A. Zhou, Y. Zhou, and D. Massatt. Convergence of the planewave approximations for quantum incommensurate systems. *arXiv:2204.00994*.
- [27] Y. Zhou, H. Chen, and A. Zhou. Plane wave methods for quantum eigenvalue problems of incommensurate systems. *Journal of Computational Physics*, 384:99–113, 2019.
- [28] K. Jiang, Q. Zhou, and P. Zhang. Accurately recover global quasiperiodic systems by finite points. *arXiv preprint arXiv:2309.13236*, 2023.
- [29] R.A. Adams and J.J. Fournier. *Sobolev spaces*. Elsevier, 2003.
- [30] H. Bohr. *Almost Periodic Functions*. Courier Dover Publications, 2018.
- [31] B.M. Levitan and V.V. Zhikov. *Almost Periodic Functions and Differential Equations*. CUP Archive, 1982.
- [32] L. Grafakos. *Classical Fourier Analysis*, volume 2. Springer, 2008.
- [33] Z. Meng, L. Wang, W. Han, F. Liu, K. Wen, C. Gao, P. Wang, C. Chin, and J. Zhang. Atomic bose–einstein condensate in twisted-bilayer optical lattices. *Nature*, 615(7951):231–236, 2023.
- [34] B. Simon. Almost periodic Schrödinger operators: a review. *Advances in Applied Mathematics*, 3(4):463–490, 1982.
- [35] J. Shen, T. Tang, and L. Wang. *Spectral Methods: Algorithms, Analysis and Applications*, volume 41. Springer Science & Business Media, 2011.
- [36] H. Liao, B. Ji, and L. Zhang. An adaptive bdf2 implicit time-stepping method for the phase field crystal model. *IMA Journal of Numerical Analysis*, 42(1):649–679, 2022.
- [37] H. A. Van Der Vorst. Krylov subspace iteration. *Computing in Science & Engineering*, 2(1):32–37, 2000.
- [38] D. S. Watkins. The matrix eigenvalue problem: GR and Krylov subspace methods. SIAM, 2007.
- [39] R.B. Lehoucq. Implicitly restarted arnoldi methods and subspace iteration. *SIAM Journal on Matrix Analysis and Applications*, 23(2):551–562, 2001.
- [40] R.B. Lehoucq, D.C. Sorensen, and C. Yang. *ARPACK Users’ Guide: Solution of Large-scale Eigenvalue Problems with Implicitly Restarted Arnoldi Methods*. SIAM, 1998.
- [41] T.G. Wright and L.N. Trefethen. Large-scale computation of pseudospectral using arpack and eigs. *SIAM Journal on Scientific Computing*, 23(2):591–605, 2001.
- [42] I. Babuška and J. Osborn. Eigenvalue Problems. *Handbook of Numerical Analysis*, 2:641–787, 1991.
- [43] C. Canuto, M.Y. Hussaini, A. Quarteroni, and T.A. Zang. *Spectral methods: Fundamentals in Single Domains*. Springer Science & Business Media, 2007.
- [44] J. Liesen and Z. Strakos. *Krylov Subspace Methods: Principles and Analysis*. Oxford University Press, 2013.
- [45] C.T. Kelley. *Iterative Methods for Linear and Nonlinear Equations*. SIAM, 1995.
- [46] Y. Saad. *Iterative Methods for Sparse Linear Systems*. SIAM, 2003.
- [47] G.W. Stewart. A Krylov-Schur algorithm for large eigenproblems. *SIAM Journal on Matrix Analysis and Applications*, 23(3):601–614, 2002.
- [48] B. Freedman, G. Bartal, M. Segev, R. Lifshitz, D.N. Christodoulides, and J.W. Fleischer. Wave and defect dynamics in nonlinear photonic quasicrystals. *Nature*, 440(7088):1166–1169, 2006.
- [49] L. Levi, M. Rechtsman, B. Freedman, T. Schwartz, O. Manela, and M. Segev. Disorder-enhanced transport in photonic quasicrystals. *Science*, 332(6037):1541–1544, 2011.